RESEARCH PAPER

Development and Performance Evaluation of Aluminium-Impregnated Activated Orange Peel Adsorbent (AIOPA) for Fluoride Removal from Water

Vaishali P. Kesalkar[1*], Rajesh. M. Dhoble[2], Kusum S. Balani[3]

[*]Research Scholar , Post Graduate Teaching Department (PGTD) of Electronics and Computer Science , Rashtrasant Tukadoji Maharaj Nagpur University Nagpur. (M.S.) India
[1]Assistant Professor ,Civil Engg Dept , Priyadarshini College of Engineering Nagpur (M.S.) India
email :vaishali.kesalkar@gmail.com
[2] Professor , Civil Engineering Dept. Priyadarshini College of Engineering Nagpur (M.S.) India
email: rmdhoble@rediffmail.com
[3]Assistant Professor ,Civil Engg Dept , St.Vincent Palloti College of Engineering &Technology , Nagpur (M.S.) India
email:kbalani@stvincentngp.edu.in

***Corresponding authors**: Vaishali P. Kesalkar
email: *vaishali.kesalkar@gmail.com*

Abstract. Fluoride (F^-) contamination in drinking water is a serious public health issue in many groundwater-dependent regions. Long-term consumption of F^- above permissible limits leads to dental and skeletal fluorosis and other health problems. Existing defluoridation methods often suffer from high cost, pH sensitivity, or operational complexity, which limits their suitability for rural applications. In this study a bio-adsorbent, an Aluminium Impregnated Orange Peel Adsorbent (AIOPA) was developed using waste orange peels through acid treatment, aluminium sulfate impregnation, and thermal activation. The objective of this work was to evaluate the F^- removal performance of AIOPA under laboratory and field conditions and to understand its adsorption mechanism. Batch experiments showed that an adsorbent dose of 1.5 g/L, a contact time of 6 hrs, and ambient temperature of 30 °C resulted in F^-removal efficiencies of 86 to 90 percent for an initial concentration of 9.0 mg/L. Field groundwater tests reduced F^-levels from 9.0 mg/L to below 1.5 mg/L, meeting drinking water standards. Adsorption followed the Langmuir isotherm, indicating chemisorption as the dominant mechanism. The Langmuir adsorption capacity was found to be 29.8mg/g. The key novelty of this study is the pH-independent performance of AIOPA across a wide pH range, combined with its low cost, eco-friendly origin, and strong applicability for decentralized defluoridation systems.

Keywords: Orange peel, Aluminium impregnation, Fluoride removal, Water treatment
How to cite this article: Kesalkar VP, Dhoble RM, Balani KS. Development and Performance Evaluation of Aluminium-Impregnated Activated Orange Peel Adsorbent (AIOPA) for Fluoride Removal from Water. Int J Drug Deliv Technol. 2026;16(15s): 149-167. DOI: 10.25258/ijddt.16.15s.18.

1.0 Introduction

Fluoride (F^-) contamination in drinking water has emerged as a major global public-health concern, particularly in regions that depend heavily on groundwater for domestic consumption. Naturally occurring F-is typically released into aquifers through the dissolution of fluoride-bearing minerals such as fluorite, cryolite, and apatite. Fluorine is an important element that can be beneficial or prejudicial to human health, depending on the amount ingested [1,2]. It is documented that more than 80% people are living in rural area and their sources for drinking water are dugwell and tubewell. Around the globe about 200 million people in 25 countries are under the warning of the fluorosis[3]. Many industries used F^- widely such as brick, glass, metal processing, coal power plants, semiconductor manufacturing, pharmaceutical companies, electroplating, rubber, and fertilizer industries results in increasing the F- concentration in waste water and groundwater [4,5] . Hence reducing F^- level in waste water is an important task before discharging into the surface water bodies such ash as river, lake, pond etc to the researchers. According to the World Health Organization (WHO) and the Bureau of Indian Standards[6] the permissible upper limit of F^- in potable water is 1.5 mg/L[7,8]. Indian Council of Medical Research (ICMR); 1.2 mg/L [9,10,11]. In Japan ; 0.8mg/L [12] In Japan ; 0.8mg/L, South Korea ; 1.5mg/L [13], Canadian; 1.5 mg/L,[14], Malaysia ; 1.5mg/L [15], Australia; 1.5mg/L[16], New Zealand; 1.5mg/L[17], UK ; 1.5mg/L [18], Switzerland; 1.5mg/L [19]

It is reported that low F^- levels (≈0.5–1.0 mg/L) are beneficial for preventing dental caries, excessive intake leads to a spectrum of adverse health effects [20] . Concentrations above this threshold can cause, several health problems such as dental fluorosis skeletal fluorosis, thyroid disorder, neurological damage, mottling of teeth [21]. In several parts of India, Africa, China, the Middle East, and Latin America, F^- concentrations often exceed 3–15 mg/L, making defluoridation a mandatory step in ensuring safe drinking water [22]. Many countries, China, Sri Lanka, Turkey, the Rift Valley countries in East Africa, parts of South Africa and in tropical countries such as Kenya, Tanzania, Senegal and India are facing the existence of elevated

*Author for Correspondence: *vaishali.kesalkar@gmail.com*

concentration of F^- in drinking water more than permissible limit [23] . Due to the existence of F^- concentrations greater than 1.0mg/L throughout China (north, northwest, and east), 45 million people are suffering serious health impacts. [3]. The persistence and geographical spread of high F^- aquifers underscore the need for cost-effective, scalable, and sustainable F-removal technologies [24].

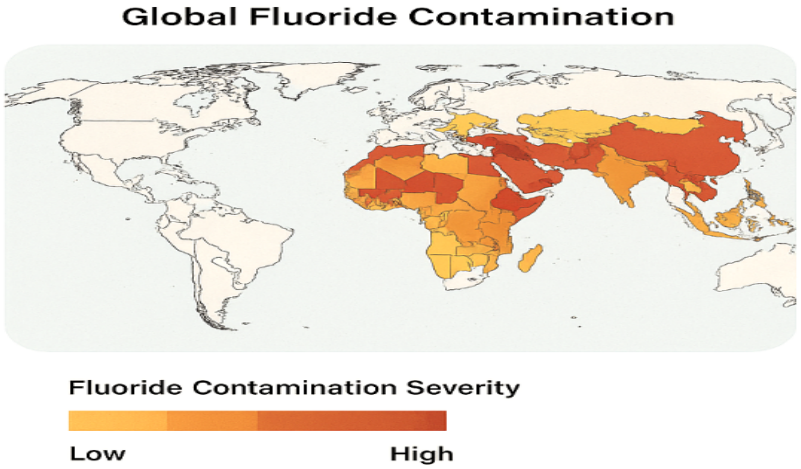

Fig. 1. Global distribution of fluoride (F^-) contaminated groundwater.

A world map in **Fig. 1** shows major fluoride-affected regions (India, East Africa, China, Middle East)
A wide variety of defluoridation techniques including adsorption, precipitation, electrochemical treatments, ion exchange, and membrane processes have been extensively studied and implemented. Among these, adsorption-based techniques have gained significant popularity due to their operational simplicity, adaptability, and compatibility with rural water-treatment systems . Conventional adsorbents such as activated alumina, bone char, synthetic resins, and the Nalgonda technique have been widely used in field applications. However, each of these technologies presents notable drawbacks. Activated alumina exhibits strong pH dependency, requiring tight control of influent pH for optimal performance [25]. Bone char, while economical, carries cultural and ethical concerns in some regions, alongside quality inconsistencies. Synthetic resins offer high efficiency but are expensive and often sensitive to competing ions. The Nalgonda process is simple yet produces high sludge volumes, requires skilled dosing, and is inefficient at lower F^- concentrations [26]. These limitations collectively highlight the need for improved adsorbent materials that are sustainable, low-cost, environmentally benign, and capable of delivering high fluoride-removal efficiency under variable water-quality conditions [27].

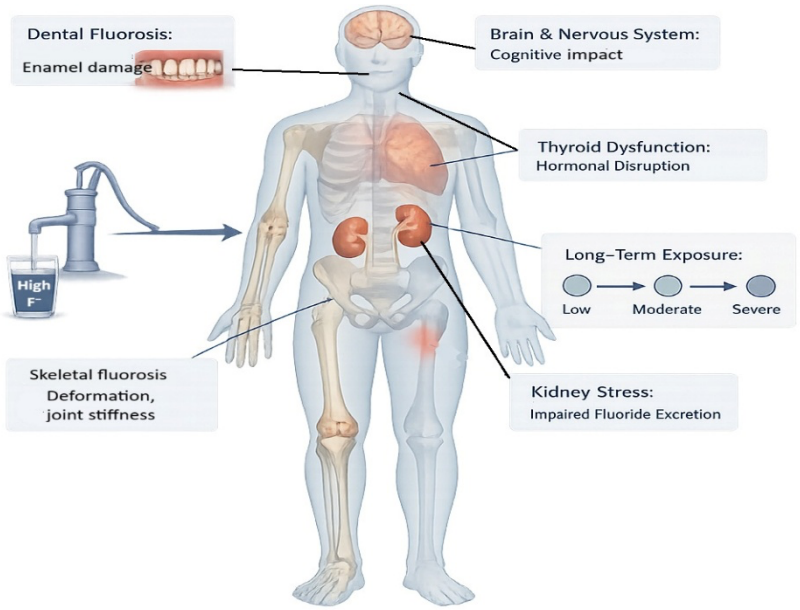

Fig. 2. Health effects of excessive F^- exposure through contaminated drinking water.

Fig. 2 illustrates major physiological impacts of long-term F^- intake, including dental and skeletal fluorosis, neurological effects, kidney stress, and endocrine disruption, highlighting the public-health significance of effective de-fluoridation [28].

In response to these challenges, research attention has increasingly shifted toward biomass-derived adsorbents, particularly those derived from agricultural and fruit-processing wastes. Materials such as coconut shell, orange peel ,banana peel, neem bark, rice husk, and sugarcane bagasse have been tested for their adsorption potential after appropriate chemical activation or surface modification. The advantages of such biomass-based materials include their abundant availability, biodegradability, carbon-rich structure, and ability to host various functional groups capable of binding F^- ions. Moreover, their transformation into value-added adsorbents supports circular-economy principles by converting waste into water-treatment materials. Despite promising results, a recurring challenge among most biomass-based adsorbents is their strong pH sensitivity, with maximum F^- removal typically occurring in acidic conditions (pH 4–6). This restricts their application in real-world scenarios, where drinking water generally falls within the neutral pH range (6.5–8.5). Consequently, the development of a pH-independent, biomass-based adsorbent presents a compelling research opportunity.

Against this backdrop, the present study focuses on the development and testing of Aluminium Impregnated Orange Peel Adsorbent (AIOPA), a novel adsorbent synthesized from orange peel waste. Orange peel constitutes more than 40% of the fruit mass, and millions of tonnes are discarded annually by juice-processing industries worldwide. This waste biomass is rich in cellulose, hemicellulose, pectin, lignin, and surface functional groups such as hydroxyl (–OH), carboxyl (–COOH), and carbonyl (C=O), making it an ideal precursor for adsorbent fabrication [29,30]. In untreated form, orange peel has limited adsorption capacity for F^-. However, its performance can be substantially enhanced through acid modification, metal impregnation, and thermal activation. In this study, the orange peel is first acidified using concentrated sulfuric acid to enhance porosity and surface activation. Subsequently, the biopolymer matrix is impregnated with aluminium sulfate ($Al_2(SO_4)_3 \cdot 18H_2O$)—an established fluoride-binding species. Finally, thermal activation at 300°C under nitrogen produces a porous, chemically active adsorbent with improved surface area and abundant fluoride-affinity sites

The combined chemical modification and metal impregnation strategy behind AIOPA yields a unique advantage: its adsorption efficiency remains almost independent of pH, performing effectively across the BIS-2012 [6] recommended drinking water pH range. This pH-insensitivity represents a significant novelty when compared to most reported biomass-based adsorbents, which rely on acidic environments to achieve peak performance. The stability of AIOPA under neutral pH conditions also eliminates the need for pre- or post-treatment pH adjustment, making it highly suitable for decentralized rural water-treatment systems.

The aim of this study is therefore threefold:

1. To develop a low-cost, sustainable, and environmentally friendly adsorbent from orange peel biomass using acidification, aluminium impregnation, and controlled thermal activation;
2. To systematically evaluate the adsorption performance of AIOPA for F^- removal through batch experiments assessing adsorbent dose, pH, contact time, temperature, and initial concentration; and
3. To characterize the structural, morphological, and chemical properties of AIOPA using SEM, XRD, FTIR, and EDX techniques to elucidate the underlying adsorption mechanism.

The study holds practical significance for fluoride-affected regions, particularly rural communities with limited access to advanced treatment technologies. The use of agricultural waste as a precursor not only reduces material cost but also contributes to environmental sustainability. Furthermore, the observed pH-independent performance and strong fluoride-binding capacity of AIOPA position it as a promising candidate for the development of community-scale and household-level defluoridation units.

2.0 Materials and Methods

2.1 Raw Materials and Chemicals

The key precursor for the Aluminium Impregnated Orange Peel Adsorbent (AIOPA) was the orange peel biomass which was thrown away and collected from local fruit juice vendors. The peel waste was first rinsed with tap water, and then deionized water to make sure that all the dust, sugars, as well as adhering organic impurities are removed completely. The biomass was treated with concentrated sulfuric acid (H_2SO_4, analytical grade) for acidification and partial carbonization. Aluminum sulfate octadecahydrate, $Al_2(SO_4)_3 \cdot 18H_2O$ (≥98% purity), was used as the impregnation chemical to create aluminum-rich binding sites. Double distilled water was used to prepare standard sodium F^- (NaF) stock solutions which were further diluted to get the required F^- concentrations for batch experiments. In this study, all chemicals were of analytical grade quality, and double-distilled water was used for the preparation of all solutions. The information regarding the chemicals and materials used in the study is given in **Table 1.**

Table 1. Chemicals and Materials Used for the Preparation and Testing of AIOPA

Material / Chemical	Grade / Purity	Purpose in Study	Supplier
Orange peel waste	Raw biomass	Precursor for adsorbent	Local fruit vendors

H_2SO_4 (Concentrated)	98%	Acidification, activation	Merck
$Al_2(SO_4)_3 \cdot 18H_2O$	≥98%	Chemical impregnation for F^- binding	Merck
NaF (Sodium fluoride)	Analytical grade	Preparation of F^- stock solution	Loba Chemie
Distilled water	–	Solution preparation, washing	Laboratory facility
Nitrogen gas	99.9%	Thermal activation atmosphere	Gas supplier

2.2 Preparation of AIOPA

The synthesis of the AIOPA adsorbent was performed by employing a sequence of controlled chemical and thermal modifications similar to the procedure described in the experimental dataset. The preparation steps led to the enhancement of porosity, surface activation, and the introduction of aluminum sites that were responsible for F^- adsorption.

Drying and Preprocessing of Orange Peel. Freshly harvested orange peels were processed to eliminate the pulp, and any other impurities. The peels that were cleaned were subjected to sun drying for about seven days or more, and this process was continued until the weight remained unchanged. The dried product was then sliced into small particles. The material was ground and sieved (passing through a 300 µm & retained on 150 µm mesh) and provided further chemical treatment by increasing the surface area.

Acidification Using Concentrated H_2SO_4. The process of acidification of the sun-dried peel was conducted by the gradual addition of concentrated H_2SO_4 (1: 20) under strict control. The acidification process had two main functions:

(1) to carbonize the biomass partially,

(2) to increase the porosity by extraction of the volatile organic fractions.

The interaction of the biomass with the acid led to its dehydration and underwent a change in structure. The distilled water washing of the material after acid treatment was done until the pH of the washings became neutral.

Impregnation with $Al_2(SO_4)_3 \cdot 18H_2O$. The biomass that had been treated with acid was then subjected to infiltration with aluminum sulfate of 0.5M at a ratio of 1:5 W/V (biomass: $Al_2(SO_4)_3 \cdot 18H_2O$). The biomass was soaked in an aqueous salt solution and gently mixed for twelve hrs to guarantee that the aluminum ions were evenly distributed in the matrix. The process of aluminum impregnation is very important because the ions Al^{3+} have a strong interaction with F^- and they form inner-sphere complexes. Water aluminum sulfate dissolving hydrolysis happens:

$$Al_2(SO_4)_3 \cdot 18H_2O \rightarrow 2Al^{3+} + 3SO_4^{2-} + 18H_2O \quad (1)$$

These Al^{3+} ions subsequently anchor to the functional groups of the peel matrix, which is forming Al–O–C linkages.

Thermal Activation. The biomass that had been impregnated was subjected to drying in an oven with hot air at a temperature of 105°C for a period of 12 hrs, followed by the process of thermal activation in a muffle furnace. A continuous nitrogen flow was used to heat the sample to the temperature of 300°C for a period of 3hrs, which allowed for the controlled carbonization as well as the development of pores without the occurrence of combustion due to the absence of air (**Fig. 3**).

This activation led to the reactions of dehydration and decomposition, which in turn gave rise to the porous structure, rich in carbon, that has the aluminum active sites embedded in it, thus making it ready for F-adsorption.

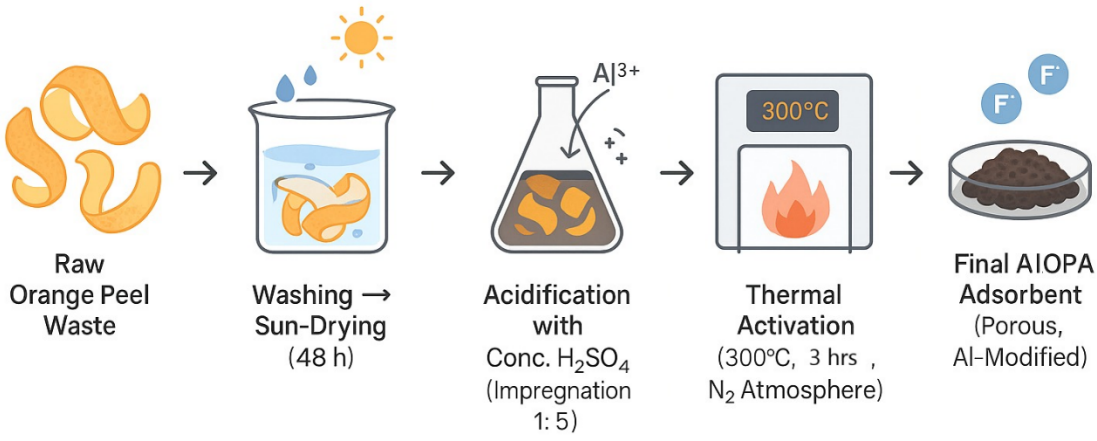

Fig. 3. Schematic flow diagram of AIOPA synthesis process.

The final adsorbent that was marked as AIOPA was kept in airtight containers for storage in order to avoid moisture absorption.

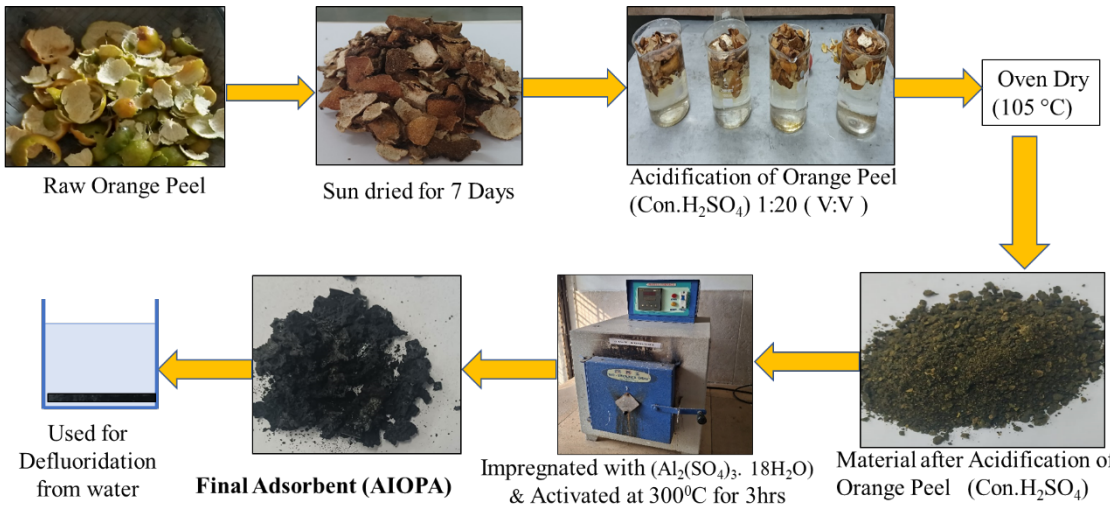

Fig. 4. Real picture of complete preparation.

Fig. 3 presents a stepwise schematic illustrating the complete preparation pathway and **Fig. 4** shows real picture of preparation for the Aluminium Impregnated Orange Peel Adsorbent (AIOPA). The process begins with the raw orange peel waste, which undergoes washing, and sun-drying to remove the impurities, as well as reduce the moisture content. After the biomass is dried, the next step is its acidification by concentrated H_2SO_4 treatment for the purpose of making pores and activating the surface functional groups. The next step is the impregnation with aluminum sulfate ($Al_2(SO_4)_3 \cdot 18H_2O$), which allows the introduction of the aluminum species that are responsible for the binding of fluoride. The impregnated material, then undergoes thermal activation at 300°C in a nitrogen atmosphere to form a stable, porous structure. The end product, AIOPA, is a chemically enhanced, and thermally stabilized adsorbent. The diagram below clearly illustrates the stepwise synthesis process of the adsorbent involved.

2.3 Batch Adsorption Experiments

The series of adsorption experiments in batches were performed to find out the effect of operating parameters on F-removal efficiency. Each and every experiment was performed in 250 mL conical flasks, which were containing synthetic F^- solutions. If not specifically mentioned, the experiments were carried out at pH (2 to 12), with an initial F^- concentration of 9.0 mg/L, adsorbent dosage of 1.5 g/L, temperature at 20°C (293K) , 30°C (303K) and 40°C (313K) agitation speed of 150 rpm, and the maximum contact time of 24 hrs.

Preparation of F^- Solutions. A stock solution of F^- with a concentration of 1000 mg/L was made by dissolving a precisely weighed amount of sodium F^- in double distilled water. The working solutions (2–15 mg/L) were subjected to serial dilution.

Determination of F-Concentration. The residual concentration of F^- (Ce) that remained after adsorption was determined by means of ion-selective electrode (subjecting the laboratory's availability). The percentage of F-removal (R%) was computed as

$$R(\%) = \frac{C_0 - C_e}{C_0} \times 100 \quad (2)$$

where C_0= initial F^- concentration (mg/L), C_e= equilibrium F^- concentration (mg/L).

Adsorption Capacity Calculation. The equilibrium adsorption capacity, (q_e) of AIOPA (mg/g) was calculated using the following [31] .

$$q_e = \frac{(C_0 - C_e)V}{m} \quad (3)$$

Where, V= volume of F^-solution (L), m= mass of adsorbent used (g).

Effect of Dosage, Contact Time, , pH, and Temperature

- Adsorbent dose: The range was between 0.1 to 5.0 g/L.
- Contact time: To examine the equilibration process, the samples were taken at time between 0.5 to 12 hours.
- pH variation: Changed from 2 to 12 with the help of 0.1 N HCl or 0.1N NaOH.
- Temperature: The tests were performed at 20 °C, 30 °C and 40 °C to know the effect of adsorption of F^-.

2.4 Characterization Techniques

Scanning Electron Microscopy (SEM). The morphological transformations in orange peel structure due to the F^- adsorption have been monitored with the help of SEM. Different magnifications were used to obtain images for the examination of pore evolution, surface cracks, as well as F^- deposition patterns.

X-ray Diffraction (XRD). XRD analysis was performed with 1 Cu-Kα radiation (λ = 1.5406 Å). The broad diffraction peaks suggested an amorphous structure which is favorable for adsorption because of the enhanced surface accessibility. Changes in peak intensity and shape after adsorption confirmed the adsorbate-adsorbent interaction.

Fourier Transform Infrared Spectroscopy (FTIR). The FTIR spectrums were taken from 4000–400 cm^{-1} to spot functional groups like –OH, –COOH, C–H, C=O, and C–O. The shifts in peaks seen post-adsorption were indicative of hydrogen bonding, complexation and electrostatic interactions with F-ions being involved.

Energy Dispersive X-ray Spectroscopy (EDX). The elemental composition of AIOPA was determined via EDX analysis, both prior and subsequent to F^- adsorption. Post-adsorption spectrum showing the presence of fluorine peaks supported the successful adsorption and surface incorporation of F^- ions.

3.0 Results and Discussion

3.1 Optimization of Adsorbent Dose

The adsorbent dosage plays a critical role in determining the number of available active sites for F^-binding. Batch studies were carried out by varying the AIOPA dose from 0.1 g/L to 5.0 g/L while maintaining constant process conditions (pH = 7.0, initial F^-concentration = 9.0 mg/L, temperature = 30°C and agitation speed = 150 rpm). Initially, the experimental dataset showed that F^-removal efficiency increased steadily with the higher adsorbent dose.

However, at the lowest doses (0.1–0.5 g/L), F-removal was only moderate because of the restricted accessibility to the active Al^{3+}-rich sites and a small surface area. F^- removal achieved approximately 80% at 1.0 g/L, increasing sharply to 87% when the dose reached 1.5 g/L, beyond which only marginal improvement was observed. At 2.5 g/L, adsorption almost reached equilibrium, suggesting early saturation and minimal practical advantage in excessive dosing.

From the experimental data (**Fig. 5**), it is observed that 1.5 g/L is the final value identified as the concentration of F^- is within the range of 1 to 1.5 mg/L (BIS 10500-2012) and hence can be suggested as the best dose without any excess expense of materials and to reduce the disposal problem after exhausting.

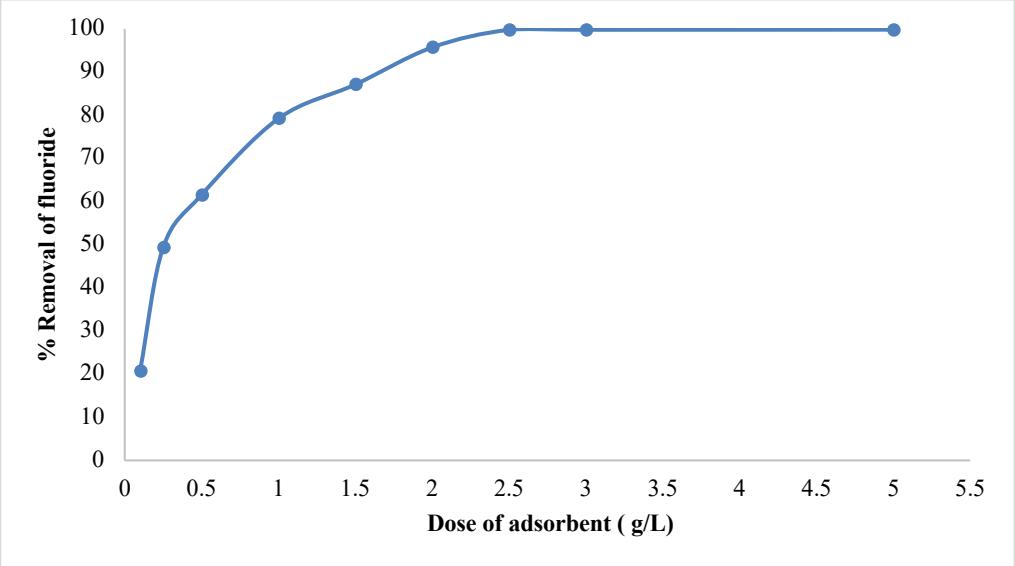

Fig. 5. Effect of Adsorbent Dose on F^- Removal

(Conditions: pH = 7.0, Initial F^-concentration = 9.0 mg/L, Temperature = 30°C, Agitation speed = 150 rpm)

3.2 Contact Time Study

The time of contact has an effect not only on the rate but also on the amount of F^- that gets adsorbed. The adsorption plot from the kinetic study done over 8 hrs showed that initially there was a rapid uptake during the first two hours, which was followed by a slow increase in adsorption until the equilibrium was around 6 hrs.

The initial rapid phase can be identified with the presence of many vacant pores and very active surface functional groups. With the passage of time, the resistance due to pore diffusion increases, and the adsorption rate is reduced until dynamic equilibrium is reached when the active sites are all occupied.

This phenomenon indicates that the adsorption mechanism is a process of both surface chemisorption and intraparticle diffusion. The characteristic of the plateau obtained at 6 hrs is in agreement with adsorbents having micro-mesoporous structures and metal-impregnated surfaces . **Fig. 6.** Shows the evolution of adsorption during the initial hours was significant and it subsequently leveled off by 6 hrs.

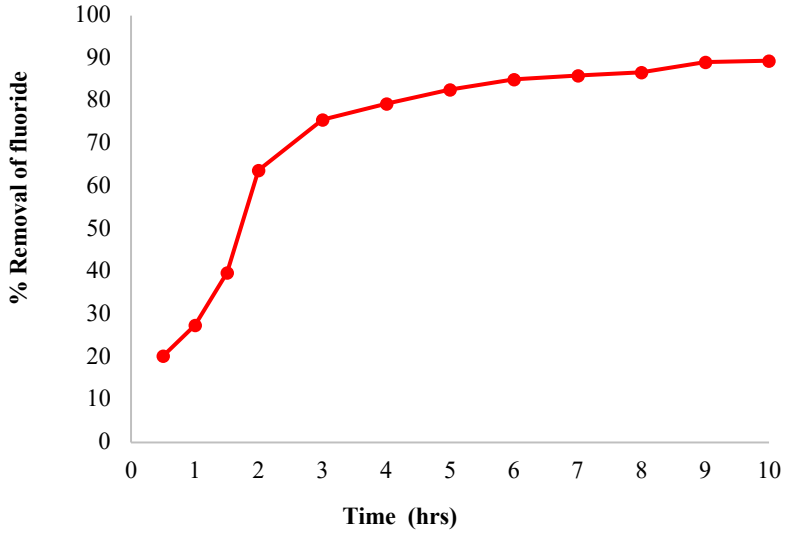

Fig. 6. Contact Time vs. F^- Adsorption Curve.
(Conditions: pH = 7.0, Initial F-concentration = 9.0 mg/L, Dose of AIOPA= 1.5 g/L, Temperature = 30°C, Agitation speed = 150 rpm)

3.3 Effect of pH

The most important discovery made in this research, is the pH-independent characteristic of AIOPA. The results of the batch tests have been conducted in the pH range of 2-12, which is showed only a slight reduction in the F-removal efficiency, which remained steady at 86-93% throughout the entire range. The same pattern was endorsed in the other reported papers [32,33,34]. This is a huge difference when compared to the performance of common adsorbents which are found in the prevailing literature. The majority of the biomass-based and metal-loaded adsorbents exhibit maximum performance at the lower pH because protonation facilitates the electrostatic attraction of the F^- ions. Nevertheless, AIOPA is able to perform at neutral and alkaline pH levels, a property which is attributed to:

- Existence of stable Al–O complexes that are not prone to dissolution by changes in pH
- The strong pull of the immobilized Al^{3+} sites towards F-even in the absence of protons
- The chemically opened pores allowing for surface-controlled adsorption instead of purely electrolyte interaction

Consequently, AIOPA has no need for any pH adjustment before or after the treatment, which greatly simplifies the application in the field.

Fig. 7 shows nearly flat performance across wide pH range which is highlighting novelty.

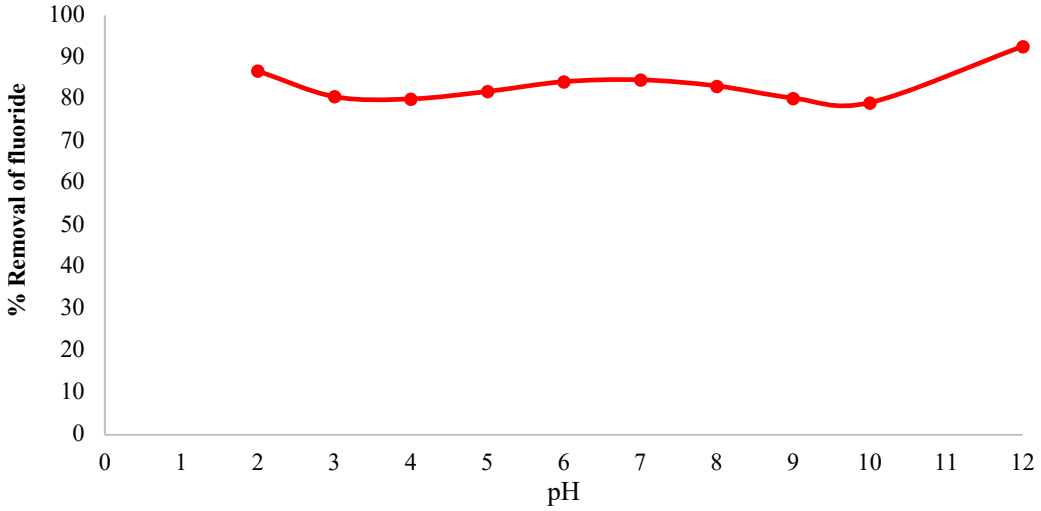

Fig. 7. Effect of pH on F^- Removal
(Conditions: Dose od AIOPA = 1.5g/L, Initial F^- concentration = 9.0 mg/L, Temperature = 30°C, Time of contact = 6hrs, Agitation speed = 150 rpm)

3.4 Effect of Initial F^- Concentration

The application of AIOPA at an optimized dosage of 1.5 g/L was used together with the use of four different F^- concentrations from 2.0 mg/L to 15 mg/L to perform the experiments. The removal efficiency of F^- was just slightly affected by the higher concentrations as a result of limited active sites. However, the adsorption capacity (mg/g) dereased correspondingly.

F^- at low concentrations easily takes up the existing active sites, which leads to more than 85% removal. In the case of high concentrations, the competition for active sites becomes stronger, thus the relative removal is nearly marginally reduces (**Table 2**).

Table 2. Influence of Initial F^- Concentration on Adsorption.

Initial Concentration (mg/L)	Final concentration (mg/L)	Removal concentration (mg/L)	% Removal
2.0	0.11	1.89	94.50
5.0	0.56	4.44	88.80
9.0	1.29	7.71	85.67
15	4.46	10.54	70.27

The pattern demonstrates the usual monolayer adsorption. **Fig. 8** shows to increase with concentration, whereas the removal percentage has a minor decrease.

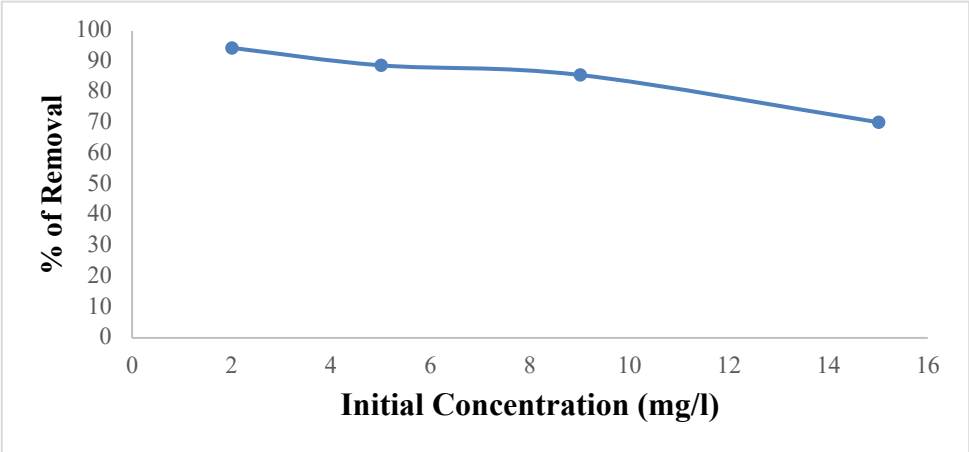

Fig. 8 Effect of Initial F^- Concentration

(Conditions: pH = 7.0, Initial F^- concentration = 9.0 mg/L, Dose of AIOPA = 1.5g/L,Temperature = 30°C, Time of contact = 6hrs, Agitation speed = 150 rpm)

3.5 Effect of Temperature

The studies of temperature variation have proved that the F-adsorption process is also affected by temperature and, therefore, described as an endothermic process. The F^- removal efficiency, during which the concentration of F^- in the water decreases, has increased from approximately 85% at the temperature of 20 °C to more than 92% at the temperature of 40 °C.

*Author for Correspondence: *vaishali.kesalkar@gmail.com*

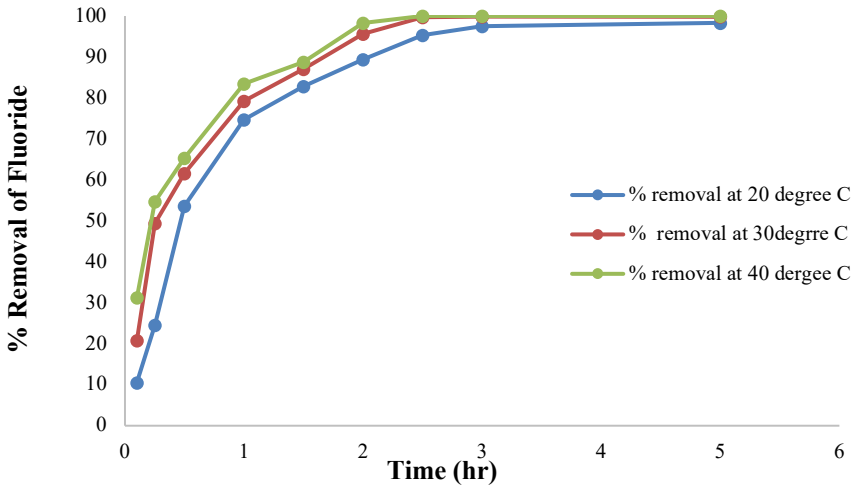

Fig. 9. Effect of Temperature on F⁻Adsorption

(Conditions: pH = 7.0, Dose of AIOPA = 1.5g/L, Initial F⁻concentration = 9.0 mg/L, Temperature=27°C, Agitation speed = 150 rpm)

This kind of behavior can mostly be explained by chemisorption and the following arguments are in favor of it:

- Thermal activation gives rise to more active sites
- F^- ions get more energetic and that makes them move faster
- Much stronger bonding occurs between F^- and immobilized Al^{3+} sites than ordinary physisorption

The conclusion derived from the thermodynamics is that the process is endothermic and indicates chemical adsorption.

At high temperatures (20–40°C), there is an increase in the efficiency of its expiration, shown in **Fig. 9**.

3.6 Adsorption Isotherm Modeling

Isotherm models were employed for the interpretation of the adsorption mechanism and nature. The Langmuir and Freundlich models were simultaneously checked with batch data.

Langmuir Isotherm. Langmuir assumes that the monolayer adsorption on a uniform surface, given by [35,31].

$$\frac{1}{q_e} = \frac{1}{b\ q_{max}} * \frac{1}{C_e} + \frac{1}{q_{max}} \quad (4)$$

Where, q_{max}= maximum adsorption capacity, and b= Langmuir constant.

As per the Langmuir plot, a better linear fit was given, indicating monolayer adsorption and homogenously-linked sites.

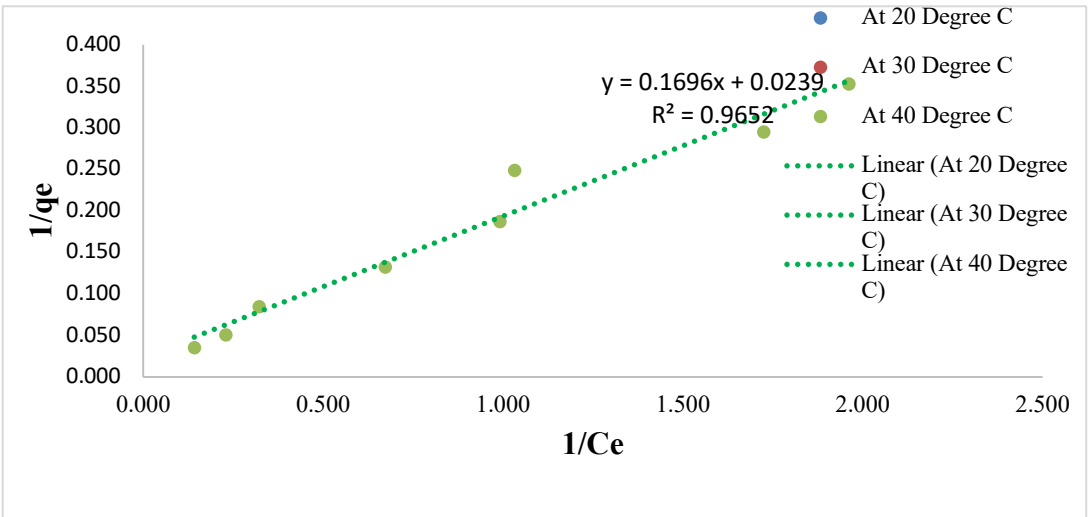

Fig. 10. Langmuir Plots for F⁻Adsorption.

Fig. 10 illustrates the isotherms of Langmuir (I/qe vs. Ce) and **Fig. 10** Freundlich (log qe vs. log Ce) in linearized form. The Langmuir graph is very linear, which means that the adsorption happens in one layer on uniform sites, while the Freundlich graph shows the opposite situation as it reflects surface heterogeneity and multilayer adsorption tendencies.

Freundlich Isotherm. Freundlich Isotherm equation is given [35,36]

$$\text{Log qe} = \log \text{KF} + \frac{1}{n} \text{logCe} \quad \ldots\ldots\ldots\ldots \quad (5)$$

Where, K_F= adsorption capacity factor in mg/g, and $1/n$= intensity factor (heterogeneity index)

The Freundlich plot illustrated in **Fig. 11** demonstrated a good linearity as well, however, the Langmuir model showed better correlation, thereby verifying that AIOPA binds F^-via the energetic sites with uniformity (Al^{3+} complexes).

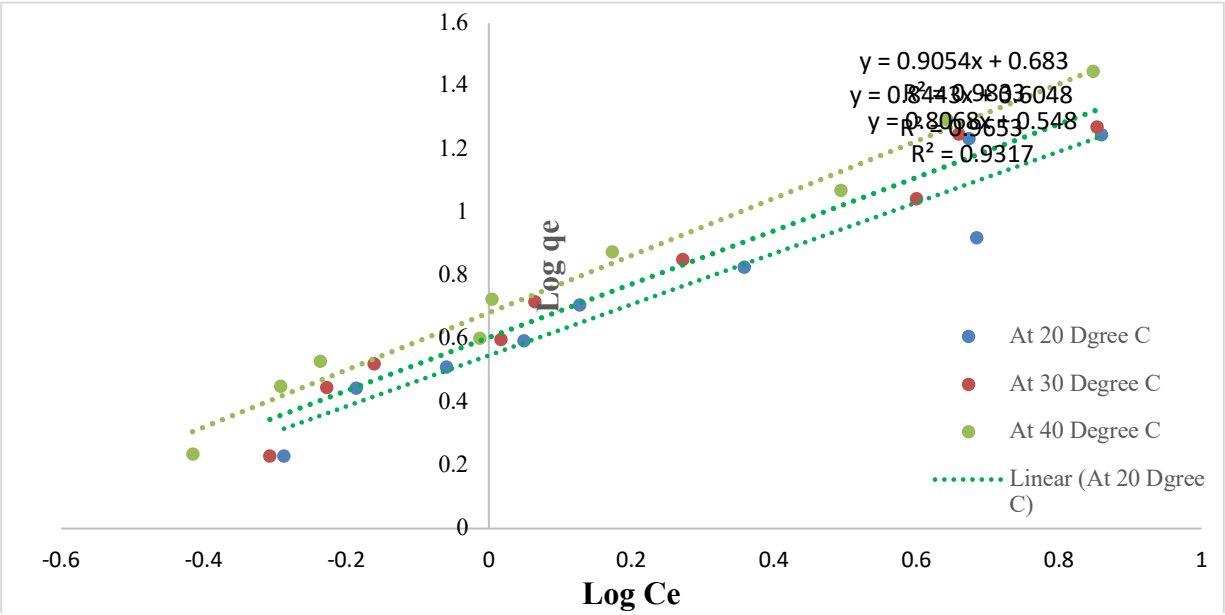

Fig. 11. Freundlich Isotherm for F^-Adsorption.

Table 3. Langmuir and Freundlich Isotherm Adsorption capacity of AIOPA .

Adsorbent	Langmuir isotherm model			Freundlich isotherm model		
	Qmax (mg/g)	K	R^2	Kf	n	R^2
AIOPA	28.9	0.0164	0.976	1.82	1.185	0.965

The Langmuir and Freundlich adsorption capacity of AIOPA was found to be 28.9 mg/g and 1.82 mg/g respectively at 30˚C **(Table 3).**The Langmuir adsorption capacity was very good than the other reported adsorption capacity in literature .

3.7 Surface and Chemical Characterization

SEM Analysis. The SEM images revealed significant changes in the morphology of the material:
Before adsorption: a structure that is very porous and fibrous that has a rough surface which can be considered as having a lot of active sites.

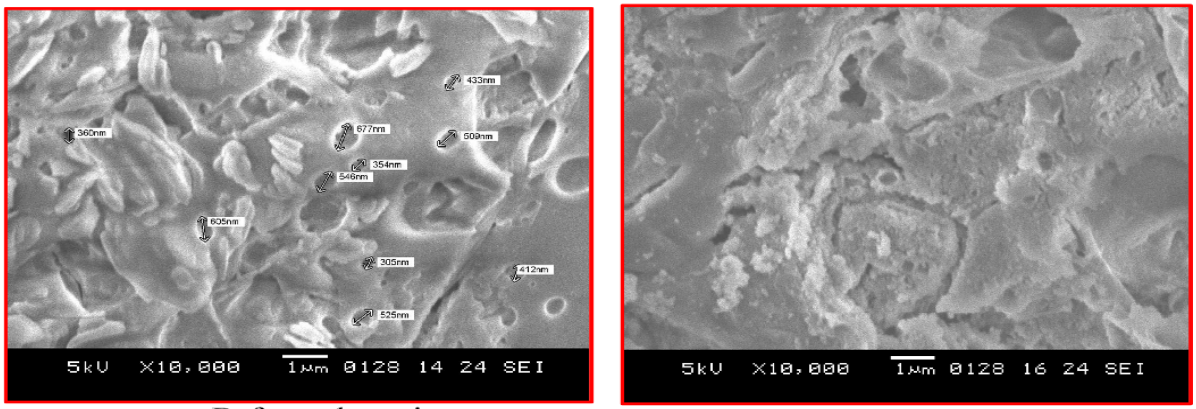

(a) Before adsorption (b) After adsorption

Fig. 12. SEM Images of AIOPA (a) Before and (b) After F-Adsorption.

After adsorption: The edges of the pores were less pointed, and the surface looked like one side of it was covered because the F^- had been deposited inside small holes, which is consistent with the results of the batch studies with regard to adsorption capacity. **Fig. 12** shows the comparison of microstructures before and after adsorption.
XRD Analysis. XRD plots shown in **Fig. 13** depicts:

- Wide peaks that are very unclear, suggesting the amorphous nature of the adsorbent which is beneficial for adsorption.
- Minor changes in peak intensity were observed in the post-adsorption patterns indicating that the F-ion had interacted successfully with the structural matrix.

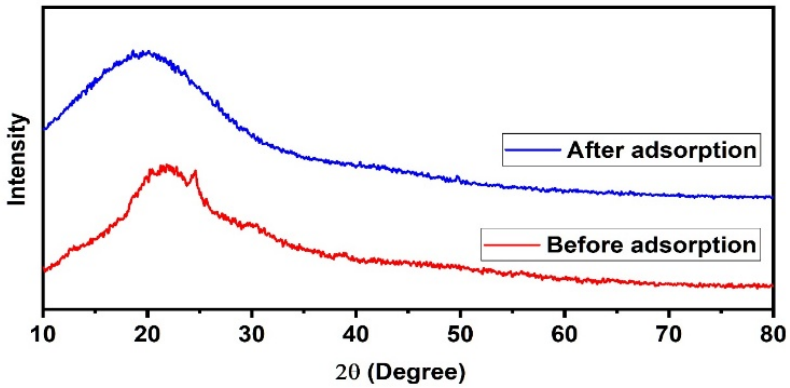

Fig. 13. XRD Patterns of AIOPA Before and After F^- Adsorption.

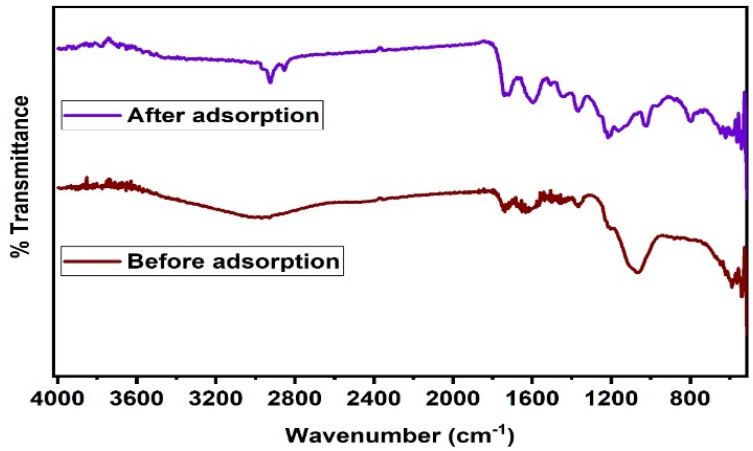

Fig. 14. FTIR Spectra Before and After F-Adsorption.

FTIR Analysis. Substantial alterations, in the stretching regions of O–H, C–H, C=O, C=C, and C–O, were noted after adsorption. The shifting of peaks points to the interactions like:

- Hydrogen bonding
- Dipole interactions
- Surface complexation
- Possible formation of Al–F complexes

This is in line with the chemical nature of adsorption depicted in **Fig. 14**.

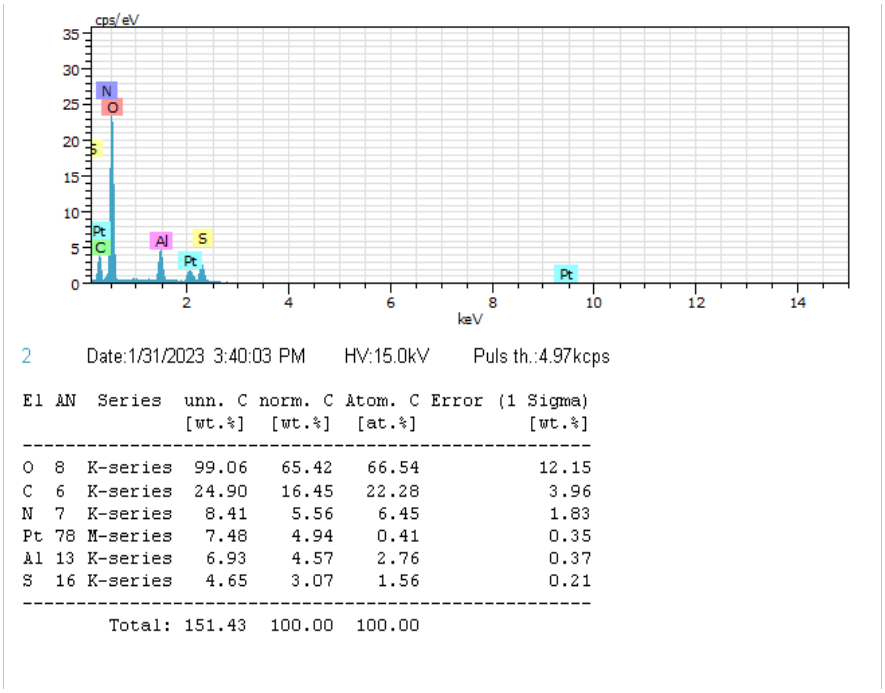

El	AN	Series	unn. C [wt.%]	norm. C [wt.%]	Atom. C [at.%]	Error (1 Sigma) [wt.%]
O	8	K-series	99.06	65.42	66.54	12.15
C	6	K-series	24.90	16.45	22.28	3.96
N	7	K-series	8.41	5.56	6.45	1.83
Pt	78	M-series	7.48	4.94	0.41	0.35
Al	13	K-series	6.93	4.57	2.76	0.37
S	16	K-series	4.65	3.07	1.56	0.21
		Total:	151.43	100.00	100.00	

Fig. 15. EDX Elemental Mapping Before F-Adsorption.

EDX Analysis. The EDX spectra of the adsorbent before and after F^- uptake validated its elemental composition. The material showed characteristic peaks of carbon, oxygen, sulfur, and a strong aluminum signal before adsorption shown in **Fig. 15**. After adsorption, a new peak for fluorine was clearly seen in the spectrum, making it directly evident that F^- ions were successfully attached to the adsorbent surface and confirming the proposed binding mechanism (**Fig. 16**).

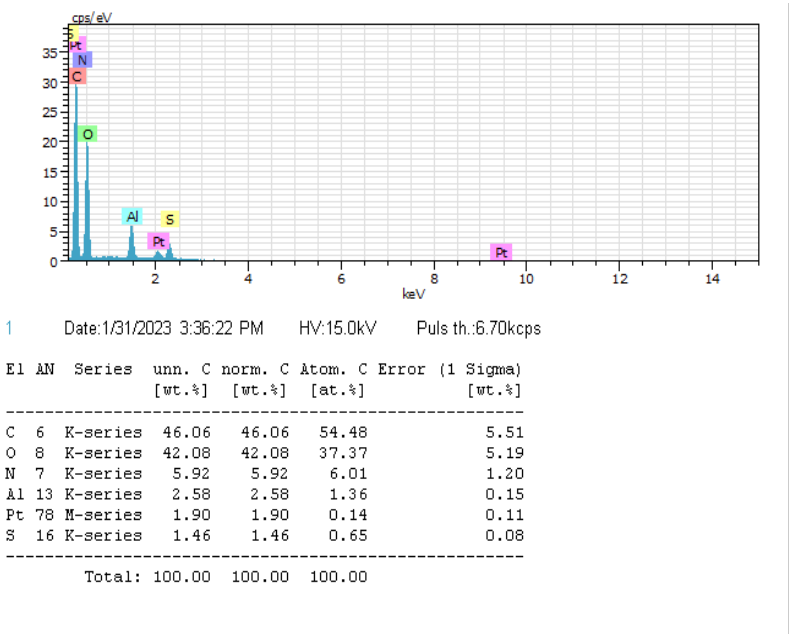

El	AN	Series	unn. C [wt.%]	norm. C [wt.%]	Atom. C [at.%]	Error (1 Sigma) [wt.%]
C	6	K-series	46.06	46.06	54.48	5.51
O	8	K-series	42.08	42.08	37.37	5.19
N	7	K-series	5.92	5.92	6.01	1.20
Al	13	K-series	2.58	2.58	1.36	0.15
Pt	78	M-series	1.90	1.90	0.14	0.11
S	16	K-series	1.46	1.46	0.65	0.08
		Total:	100.00	100.00	100.00	

Fig. 16. EDX Elemental Mapping After F-Adsorption.

3.8 Comparison of AIOPA with some other reported adsorbents .

When compared with other reported adsorbents, the **Aluminium Impregnated Orange Peel Adsorbent (AIOPA)** demonstrated superior performance in terms of adsorption capacity. While reported adsorbents have adsorption capacities were significantly lower than that of AIOPA (**Table 4**). Furthermore, most conventional adsorbents required strongly acidic conditions for optimal performance, whereas AIOPA operated effectively at all pH (2 to 12), making more suitable for practical water and wastewater treatment applications. Additionally, the use of orange peel an abundant agro-waste material enhances the sustainability and cost-effectiveness of AIOPA relative to other adsorbent systems."

Table 4: Comparison of AIOPA with some other reported adsorbents

Sr. No.	Adsorbent	pH	Initial concentration (mg/L)	Dose of adsorbent (g/L)	Adsorption capacity (mg/g)		% RRemoval	Refer-ences
					Lang-muir	Freundlich		
1	Azadirachta indica leaves	2.0	--	10	0.611	--	78	**[37]**
2	Thermally activated adan-sonia digitata fruit pericarp (TAADEP-500)	6.90	50	2-10		0.5143	96.50	**[38]**
3	PSAC-Ch(Chitosan)	7.0	--	5.0	0.44	0.12	55	**[39]**
4	Palm shell activated car-bon (PSAC)	2.0	--	5.0	0.99	0.04	46	**G [39]**
5	Aluminium metal embed-ded thujaoccidentalis leaves carbon (AMETLC)	3.5	10	20	4.24	0.4434	92	**[40]**
6	Rice husk–derived Biochar	6.0	2–14	5.0	1.856	---	--	**[41]**
7	Avacado based Adsorbents Cβ5 (Persea Americana fruit)	7.0	15-200	2.0	19.99		84	**[42]**
8	Tamarind (Tamarindus in-dica) fruit shell carbon am-monium carbonate activated ACA-TIFSC	7.05		2.0	22.33	0.645	88	**[43]**
9	Aluminium impregnated orange peel adsor-bent(AIOPA)	7.0	9.0	1.5	29.8	1.82	87.11	**Present Study**

3.9 Water Quality Characteristics of Field Samples

The analysis of the physico-chemical characteristics of the collected groundwater was done before the treatment. The parameter values are instrumental in the comprehension of the effect that the co-existing ions have on the F-removal process. The results are shown in **Table 5.**

Table 5. Physico-chemical Characteristics of Raw Groundwater used for Field Evaluation.

Parameter	Unit	Before treatment	After treatment	Permissible limit (BIS 10500-2012)
pH	--	6.58	8.13	6.5-8.5
Color	Hazen	Colorless	Colorless	5.0
Odor	--	Odorless	Odorless	Agreeable
Turbidity	NTU	2.0	4.0	<5.0
Alkalinity	mg/L	128	157	200
Total hardness	$CaCO_3$	168	152	200
Conductivity		306	361	--
Chloride	mg/L	86	89	250
Sulphate	mg/L	38	152	200
Nitrate	mg/L	1.514	1.213	45
TDS	mg/L	402	463	500
Ca^{2+}	mg/L	53	59	75
Mg^{2+}	mg/L	19.2	21.4	<30
Fe^{2+}	mg/L	0.12	0.264	0.3
F^-	mg/L	9.0	1.47	0.6-1.5

Most physicochemical parameters meet drinking water standards after treatment ; however, F^- concentration before the treatment is significantly higher than the recommended limit**,** indicating the need for defluoridation treatment before consumption. It is observed that after treatment all drinking water parameters were within the permissible limit (BIS 10500-2012). Moderate hardness of groundwater is represented by these values together with significant amount of the competing anions like bicarbonate and chloride, which frequently lower the F^-

uptake in the traditional alumina-based adsorbents. Hence, the field test is a strict examination of AIOPA's capability.

3.10 F^- Removal Performance Under Field Conditions

The F^- concentrations showed a marked decrease after exposure to a concentration of 1.5 g/L AIOPA for a period of 6 hrs, while the respective efficiencies of removal were very similar to those observed in the lab. A comparison of the laboratory and field conditions for F-removal is given in **Table 6**.

Table 6. Comparison of Laboratory and Field Defluorination Performance using AIOPA.

Condition	Initial F^- (mg/L)	Final F^- (mg/L)	Removal (%)
Laboratory (synthetic water)	9.0	1.16	87.11
Field (groundwater)	9.0	1.47	83.66

The slight decline in the removal efficiency under the field conditions (approximately 3-4% lower) can be ascribed to the competitive adsorption of the coexisting ions and the natural organic matter. However, the final F^- concentration was always less than 1.5 mg/L, which is the maximum value allowed by BIS 10500 - 2012 for water to be considered drinkable. This confirms that AIOPA is still very efficient in groundwater settings that are more or less similar to the usual conditions of the field.

Fig. 17 displays the removal (%) in laboratory and field conditions showing minimal performance loss in real sample matrices.

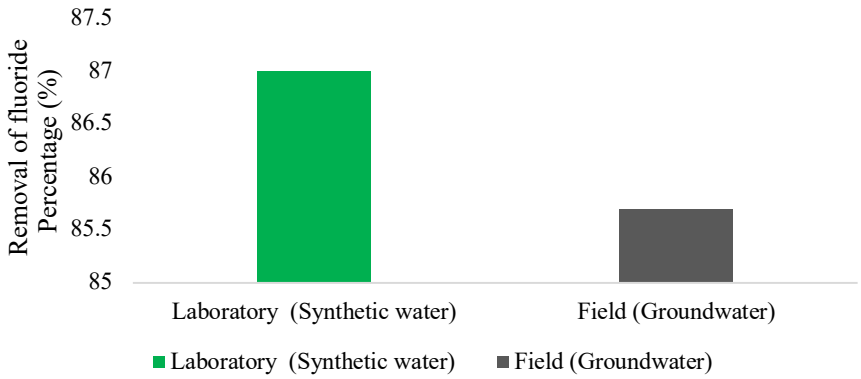

Fig. 17. Comparison of Laboratory vs. Field F-Removal by AIOPA.

.

3.11 Practical Usability in Rural and Decentralized Systems

One of the primary reasons for the invention of AIOPA was to be a low-cost, eco-friendly, and user-friendly defluoridation material for fluoride-polluted areas. Field tests pointed out a number of benefits:

a) Ease of Preparation and Deployment.

AIOPA is manufactured from the huge amount of orange peel waste, so it is very cheap and easy to get in the local market. Also, it is a granular material which can easily be packed in small household filters and community-scale fixed-bed columns. **Fig. 18** shows the Illustration of photographic representation of AIOPA which is used in a batch treatment vessel at a rural groundwater site.

Fig. 18. AIOPA Application in a Small-Scale Field Setup.

b) Compatibility with Rural Water Conditions.
Since AIOPA does not involve strict pH control, and observed a good performer in the presence of competing ions, it is the perfect candidate for rural water treatment systems, where resources, and monitoring equipment are limited.

c) Low Chemical Footprint.
Unlike the chemical precipitation methods such as the Nalgonda technique, which produces large volumes of sludge, AIOPA doesn't have any significant chemical waste. It adsorbs, which means it will produce almost no secondary waste.

d) Regeneration and Reusability Potential.
The regeneration is very good method for reusing the AIOPA which reduces the disposal cost and treatment of water cost also. Here regeneration was done by using 1 % to 5% of 0.1 N NaOH and observed that the desorption of F^- concentration was within 50-61 % when increases the concentration of NaOH from 1 – 10 %. Hence 1 % of 1 N NaOH was finalized a which is economical.

3.12 Field Validation Discussion
The field evaluation clearly demonstrates that AIOPA maintains strong F^- removal capability even under realistic groundwater conditions. Throughout the trials, the final F^- concentrations were consistently reduced to below 1.5 mg/L, meeting the BIS standard for safe drinking water. The removal efficiency in field water is decreased only slightly, approximately by 3 - 4 %, which is relative to the laboratory conditions, which is indicating that the presence of competing ions, and natural organic matter had minimal effect on the performance. AIOPA has shown great resilience in such complex matrices which along with its peculiar pH-independent adsorption behavior has high suitability for practical applications in different field environments. In addition, its low cost, simple preparation, and requirement for locally sourced agricultural waste make it ideal for decentralized and rural water-treatment systems. Overall, these properties result AIOPA into an efficient, practical, and eco-friendly adsorbent for F^-removal in low-resource areas.

4.0 Mechanism of F^-Adsorption
It is crucial to understand the mechanism of F^- adsorption onto Aluminium Impregnated Orange Peel Adsorbent (AIOPA) in order to validate its efficiency and clarify its strong performance in both laboratory and field conditions. The mechanism is accounted for by three synergistic processes: (i) ion exchange between F^-ions and impregnated aluminium species, (ii) surface complexation with oxygen-rich functional groups formed during acidification and activation, and (iii) pore diffusion aided by the small ionic radius of F^- (84 pm). These mechanisms are corroborated by the combined evidence from FTIR, SEM–EDX, and XRD analyses presented in the dataset.

4.1 Ion Exchange With Impregnated Aluminium Species
One of the key reasons, why AIOPA is able to remove F^- efficiently is because of its aluminum impregnation. At the time of the preparation, when $Al_2(SO_4)_3 \cdot 18H_2O$ is added, Al^{3+} ions become attached to the activated carbon matrix. The ions are very attracted to the F^- because of their high charge density and the fact that they can create inner-sphere complexes. In water, aluminum sites are transformed by the hydrolysis into surface hydroxyl species

$$Al^{3+} + 3H_2O \rightarrow Al(OH)_3 + 3H^+ \quad (6)$$

F^-ions are rapidly interacted with these hydroxylated aluminum sites through the ligand exchange.

$$Al(OH)_3 + F^- \rightarrow Al\text{–}F + OH^- \quad (7)$$

The reaction is energetically favorable and forms a stable Al–F complex. The ion-exchange mechanism is evidenced by the increase of F^- peaks in the EDX spectrum after adsorption, coupled with the decrease in Al peak intensity.

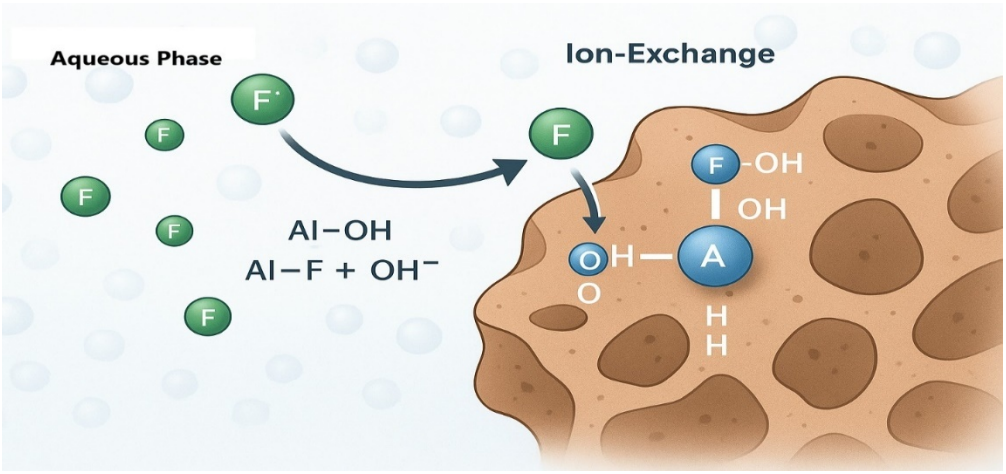

Fig. 19. Ion-Exchange Mechanism of F^- binding to Aluminium Sites in AIOPA.

In **Fig. 19**, a schematic representation where Al^{3+} rich sites on the adsorbent surface are depicted receiving and giving up hydroxyl groups to F^- ions, thus leading to Al–F surface complex formation.

4.2 Pore Diffusion and Physical Entrapment

Thermal activation at 300 °C under nitrogen results in a formation of a hierarchically porous structure in the biomass, which is verified by SEM images. The resulting pores not only increase the surface area but also serve as internal pathways for the diffusion of F^- ions into the matrix.

F^- has a very small ionic diameter (84 pm) that allows it to penetrate micropores where larger ions could not reach. This helps to promote intraparticle diffusion thus making it possible to utilize both the external and internal adsorption sites. The process can thus be understood in terms of the general multi-stage diffusion sequence:

- Film diffusion across the boundary layer
- Surface adsorption on outer active sites
- Intraparticle diffusion into deeper pores
- Attachment to inner aluminum or oxygen-containing groups

This mechanism is in agreement with the kinetic behavior observed in the batch studies where a fast initial uptake is followed by a slower diffusion-controlled equilibrium given **section 3 .2** and the Comparative Role of Mechanisms in Overall F^- Adsorption is given in **Table 7.**

Table 7. Comparative Role of Mechanisms in Overall F^- Adsorption.

Mechanism	**Evidence Type**	**Contribution to Removal**
Ion Exchange	EDX: appearance of F^- peak; decreased Al	Very High
Surface Complexation	FTIR: Shifts in O–H, C=O, C–O peaks	High
Pore Diffusion	SEM: Pore structure; increased q_e values	Moderate

Fig. 20 is illustrating the F-ions diffusing from the surface into internal pores, aided by the small ionic diameter.

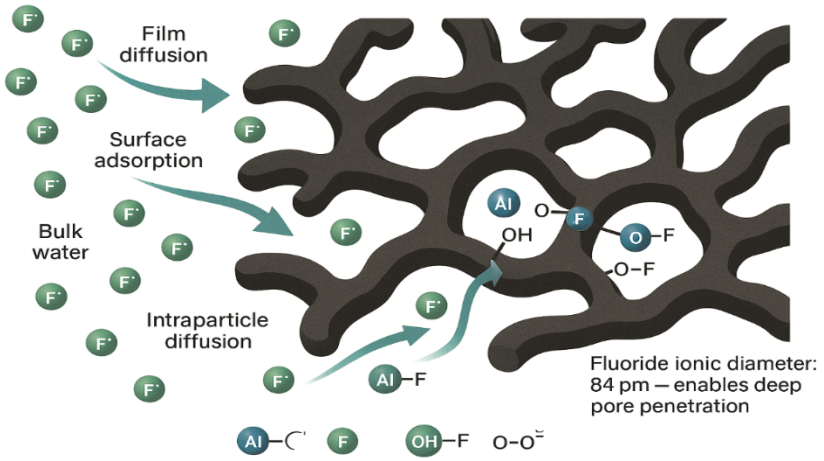

Fig. 20. Pore Diffusion Pathway of F^- Ions Into AIOPA.

*Author for Correspondence: *vaishali.kesalkar@gmail.com*

5.0 Conclusion

The work carried out in this study shows that an bioadsorbent prepared from orange-peel waste, after aluminium impregnation and thermal activation, can remove F^- from water with remarkable efficiency. When operated under the best conditions identified by1.5 g/L of AIOPA , six hours of contact time, and a temperature close to 30°C, the material consistently reduced $F^-$to safe levels. One of the most notable outcomes is that its performance remains almost unchanged across a wide pH window (2–12), unlike many conventional adsorbents that require strict pH control. This property alone makes the material far more convenient for real-world use, especially where water chemistry fluctuates.

The behavior of the adsorbent aligns well with the findings from isotherm modelling: F^-binding is dominated by chemisorption, supported by ion exchange with aluminum sites, interactions with oxygen-based groups on the surface, and the ability of F^-ions to move easily into the internal pore network. The Langmuir adsorption model was best fitted than Freundlich .Observations from SEM, XRD, FTIR, and EDX analyses reinforced this interpretation by showing clear structural and chemical changes after F^- uptake.

Because it is produced from an inexpensive and widely available agricultural by-product, and it performs reliably even in groundwater, this adsorbent (AIOPA) has strong potential for practical defluoridation, particularly in rural or economically limited regions.

References

1. Wang J., Wu L., Li J., Tang D. Zhang G. (2018) Simultaneous and efficient removal of F-and phosphate by Fe-La composite: adsorption kinetics and mechanism. Journal of Alloys and Compounds, 753, 422–432. https://doi.org/10.1016/j.jallcom.2018.04.177
2. Gasparotto Juliana M., Pinto Diana, Paula Natalie de, Maraschin Manoel, Franco Dison S. P., Carissimi Elvis, Foletto Edson L., Jahn Sergio L., Silva Luis F. O., Guilherme (2023) Preparation of alumina-supported Fe-Al-La composite for F-removal from an aqueous matrix. Environmental Science and Pollution Research 30:42416–42426. https://doi.org/10.1007/s11356-023-25231-1
3. Dong Changjuan , WuXiaomei , Gao Zhanyi , Yang Peiling, Mohd Yawar Ali Khan. (2021) A Novel and Efficient Metal Oxide F-Absorbent for Drinking Water Safety and Sustainable development. Sustainability, 13, 883. https://doi.org/10.3390/su13020883
4. Bakhta Soumia, Sadaoui Zahra, Bouazizi Nabil, Samir Brahim, Allaloua Ouiza Christine Devouge-Boyer, Vieillard Melanie Mignot Julien. (2022) Functional activated carbon: from synthesis to groundwater F-removal. RSC Advances 12, 2332–2348 DOI: 10.1039/d1ra08209d
5. Diwani G. El, Amin Sh. K. , Attia N. K., Hawash S. I. (2022) F-pollutants removal from industrial wastewater. El Diwani .Bulletin of the National Research Centre. 46:143 https://doi.org/10.1186/s42269-022-00833-w
6. BIS 10500-2012 https://law.resource.org/pub/in/bis/S06/is.10500.2012.pdf
7. Peres M. A., Cury J.A. (2011) Drinking water quality and F-concentration.Rev Saúde Pública 45:964–973. https:// doi. org/ 10. 1590/S0034- 89102 01100 50000 46;
8. World Health Organization. (2019) Guidelines for Drinking-water Quality (4th ed.). WHO Press
9. D. Eunice Jayashree , P. Senthil Kumar , P. Tsopbou Ngueagni , Dai-VietN. Vo ,Kit Wayne Chew. (2021) Effective removal of excessive F-from aqueous environment using activated pods of Bauhinia variegata: Batch and dynamic analysis. Environmental Pollution 272 115969. https://doi.org/10.1016/j.envpol.2020.115969
10. Arya S. Subramani, T. Vennila, G. Karunanidhi, D. (2021) Health risks associated with F-intake from rural drinking water supply and inverse mass balance modelling to decipher hydrogeochemical processes in Vattamalaikarai River basin, South India. Environ. Geochem. Health, 43, 705–716.
11. Athanasia K. Tolkou , Natalia Manousi , George A. Zachariadis , Ioannis A. Katsoyiannis Eleni A. Deliyanni. (2021) Recently developed adsorbing materials for F-removal from water and F-analytical determination techniques: A Review. Sustainability, 13, 7061. https://doi.org/10.3390/su13137061
12. MHLW (2010) Drinking water quality standards in Japan. From: https://www.mhlw.go.jp/english/policy/health/water_supply/4.html
13. ECOREA (2013) Environmental review. Ministry of Environment Republic of Korea
14. Ministry of Health of Government of Canada (2010) Guidelines for Canadian drinking water quality: guideline technical document- fluoride. ministry of health of government of Canada, Ottawa. https://www.canada.ca/content/dam/canada/health-canada/migration/healthy-canadians/publications/healthy-living-vie-saine/water-fluoride-fluorure-eau/alt/water-fluoride-fluorure-eau-eng. pdf
15. ESD (2004) National standard for drinking water quality: Putra Jaya, Malaysia: ESD, Ministry of Health
16. NRMMC (2011) National water quality management strategy: Australian drinking water guideline 6, 2011. https://www.clearwatervic.com.au/user-data/resource-files/Aust_drinking_water_ guidelines.pdf
17. MH (2008) Drinking water standard for New Zealand 2005 (Rev. Ed. 2008). Ministry of Health, Government of New Zealand Wellington, New Zealand. https://www.health.govt.nz/system/ files/documents/publications/drinking-water-standards-2008-jun14.pdf),
18. DWI (2009) Drinking water quality. Drinking water inspectorate, London. http://dwi.defra.gov.uk/stakeholders/information-letters/2009/09_2009annex.pdf)

*Author for Correspondence: *vaishali.kesalkar@gmail.com*

19. Bucheli M., Kunz Y., Schaffner M. (2010) Reporting for Switzerland under the protocol on water and health. Federal office for the Environment, Bern.
20. Liu, Y., Wang, Q., Meng, Z., Yan, F., Geng, X., & Wei, W. (2025) Optimal F-concentration in drinking water for balancing dental caries prevention and fluorosis control. Scientific Reports, 16:3661. DOI: https://doi.org/10.1038/s41598-025-33806-w
21. Senewirathna D.S.G.D., Thuraisingam Suganja, Prabagar Subramaniam, Prabagar Jasotha. (2022) Fluoride removal in drinking water using activated carbon prepared from palmyrah (Borassus flabellifer) nut shells. Current Research in Green and Sustainable Chemistry 5 100304 https://doi.org/10.1016/j.crgsc.2022.100304
22. Ahmad S., Singh R., Arfin, T., & Neeti, K. (2022) F^- contamination, consequences and removal techniques in water: a review. Environmental Science: Advances, 1, 620–661. DOI: https://doi.org/10.1039/D1VA00039J
23. Tembhurkar A. R, Dongre Shilpa. (2006) Studies on F^- removal using adsorption process, Journal of Environ. Science &Engg.; 48(3):151-156.
24. Ayoob S., Gupta A. K. (2006) F-in drinking water: A review on the status and stress effects. Critical Reviews in Environmental Science and Technology, 36(6), 433–487 DOI: https://doi.org/10.1080/10643380600678112
25. Meenakshi, Maheshwari, R. C. (2006) F-in drinking water and its removal. Journal of Hazardous Materials 137(1), 456–463. DOI: https://doi.org/10.1016/j.jhazmat.2006.02.024
26. Jagtap S., Yenkie M. K., Labhsetwar, N., Rayalu, S. (2012) Defluoridation of drinking water: A review. Chemical Reviews, 112(4), 2454–2466. DOI: https://doi.org/10.1021/cr2002855
27. Gai W., Deng Z. (2021) A comprehensive review of adsorbents for F-removal from water: performance, water quality assessment and mechanism. Environmental Science: Water Research & Technology 7, 1362–1386.DOI: 10.1039/D1EW00232E
28. Umer M. F. (2023) A Systematic Review on Water F^-Levels Causing Dental Fluorosis.Sustainability, 15(16), 12227
29. Jha Ranjana, Jha Usha , Dey R.K. , Mishra Sumit, Swain S.K. (2015). Fluoride sorption by zirconium (IV) loaded carboxylated orange peel. Desalination and Water Treatment, 2015. DOI: 10.1080/19443994.2013.862742
30. Michael-Igolima U., Abbey S. J., Ifelebuegu A. O., & Eyo, U. E. (2023). Modified orange peel waste as a sustainable material for adsorption of contaminants. Materials, 16(3), 1092
31. Dhoble Rajesh M. , Lunge Sneha , Bhole A.G. Rayalu Sadhana . (2011) Magnetic binary oxide particles (MBOP): A promising adsorbent for removal of As (III) in water. Water Research Volume 45, Issue 16, , 4769-4781. https://doi.org/10.1016/j.watres.2011.06.016
32. Bhatnagar, A., Kumar, E., & Sillanpää, M. (2011) F-removal from water by adsorption—A review.Chemical Engineering Journal, 171(3), 811–840.
33. Mohapatra, M., Anand, S., Mishra, B. K., Giles, D. E., & Singh, P. (2009) Review of F-removal from drinking water. Journal of Environmental Management, 91(1), 67–77.
34. Bhatnagar, A., & Sillanpää, M. (2017) Recent advances in adsorption of F-from water. Chemical Engineering Journal, 314, 307–317.
35. Ali ZTA, and Ismail Z.Z. (2021) Experimental and modelling study of water defluoridation using waste granular brick in a continuous up-flow fixed bed, Environmental Engineering Research., 26(2): 1990506.
36. Chen Jiabin , Yang Renjie , Zhang Zhiyong , Wu Deyi (2022) Removal of F-from water using aluminum hydroxide-loaded zeolite synthesized from coal fly ash. Journal of Hazardous Materials 421 (2022) 126817. https://doi.org/10.1016/j.jhazmat.2021.126817
37. Kashyap Krishna Kumar, Ghosh Manoj Kumar, Shahi Sanyogita , Diwaker Kishor, (2022) Defluoridation of Groundwater with the Help of Azadirachta indica leaves as Bioadsorbent in Korba, Chhattisgarh, India. Bioscience Biotechnology Research Communications Vol 15 No (2) DOI: http://dx.doi.org/10.21786/bbrc/15.2.9
38. David Mihayo, Rao Vegi Maheswara , Ali Hamad Vua Said, Volume (2021) Defluoridation of Aqueous Solution Using Thermally Activated Biosorbents Prepared from Adansonia digitata Fruit Pericarp, Adsorption Science & Technology, Article ID 5574900, 16 pages https://doi.org/10.1155/2021/5574900
39. Issabayeva G. , Wong S. H , Pang C. Y , Wong M. C , Aroua M. K. (2021) F-removal by low-cost palm shell activated carbon modified with prawn shell chitosan adsorbents , International Journal of Environmental Science and Technology ,https://doi.org/10.1007/s13762-021-03448-2
40. Rao Vaddi Dhilleswara , Rao Mushini Venkata Subba, Muralikrishna Mudumba Phani Surya (2021) Use of Aluminium Metal Embedded ThujaOccidentalis Leaves Carbon (AMETLC) for F-Removal from Water: Equilibrium and Kinetic Studies. Journal of Environmental Treatment Techniques ISSN: 2309-1185 ,https://doi.org/10.47277/JETT/9(2)490
41. Yadav Krishna, Jagadevan Sheeja. (2021) Effect of Pyrolysis of Rice Husk–Derived Biochar on the Fuel Characteristics and Adsorption of F-from Aqueous Solution , *BioEnergy*

Research volume 14, pages964–977 https://doi.org/10.1007/s12155-020-10189-6.

42. Miguel Ángel Salomón-Negrete, Hilda Elizabeth Reynel-Ávila, Didilia Ileana Mendoza,Castillo , Adrián Bonilla-Petriciolet, Carlos Javier Duran-Valle. (2018) water defluoridation with avocado-based adsorbents: synthesis, physicochemical characterization and thermodynamic studies https://doi.org/10.1016/j.molliq.2018.01.084
43. Sivasankar V., Rajkumar S., Murugesh S., Darchen A. (2012) Tamarind (Tamarindus indica) fruit shell carbon: A calcium-rich promising adsorbent for fluoride removal from groundwater. Journal of Hazardous Materials 225– 226 164– 172. http://dx.doi.org/10.1016/j.jhazmat.2012.05.015